Realistic Skeletal Muscle Deformation using Finite Element Analysis

ROBSON LEMOS[1], MARCELO EPSTEIN[2], WALTER HERZOG[3], BRIAN WYVILL[1]

[1]Department of Computer Science*
{lemos,blob}@cpsc.ucalgary.ca
[2]Department of Mechanical Engineering*
epstein@enme.ucalgary.ca
[3]Faculty of Kinesiology*
walter@kin.ucalgary.ca
*The University of Calgary, 2500 University Drive N.W., Calgary, AB, Canada T2N 1N4

Abstract. We present a computational model to simulate the skeletal muscle deformation during muscle contraction. This model includes a detailed description of the skeletal muscle architecture, non-linear properties of muscle tissue, novel features in the active muscle constitutive equations, and geometric constraints that can be enforced through Lagrange multipliers. The proposed muscle model predicts fibre forces based on the principle of virtual work, along with appropriate geometric constraints using a non-linear finite element analysis. This computational model introduces methods to produce realistic skeletal muscle deformation to be used in computer animation applications, and to study muscle function in biomechanical applications. Our model is sufficiently general to be applied in other non-linear soft tissues with different material properties. In order to exemplify its generality, the model is applied to different structural arrangements of individual skeletal muscles.

1 Introduction

Skeletal muscles deform in response to contraction of muscle fibres. The underlying structure of the skeletal muscle is determined by the arrangement of the contractile elements (muscle fibres) within a muscle (Figure 1). In nature, the arrangement of muscle fibres within a muscle, and the deformations during muscle contraction, have many variations. For example, if muscle fibres are arranged in parallel to the long axis of the muscle, contraction causes a bulging. However, if muscle fibres are arranged at a distinct angle to the long axis of the muscle, contractions causes no bulging but a parallel sliding of the top aponeurosis (thin layer of connective tissue within a muscle; Figure 1) relative to the bottom one. The macroscopic arrangement of muscle fibres makes up the architecture of skeletal muscle. According to Lieber and Fridén [14], muscle architecture is a primary determinant of muscle function, and the understanding of this structure-function relationship is of great practical importance. The proposed muscle model takes into account the mechanical aspects of this structure-function relationship in order to produce realistic skeletal muscle deformation. In this context, the main contribution of this research for computer graphics is that we have developed a model of skeletal muscle general enough to accommodate different muscle fibres arrangements. With this model we can produce realistic deformation of different muscle architectures of skeletal muscles and deformation of other non-linear, soft tissues with different material properties.

In this study, we introduce methods to produce realistic skeletal muscle deformation that are sufficiently general to be used in computer animation applications, and sufficiently accurate to study muscle function in biomechanical applications. In computer animation, given the kinematics of an articulated figure (e.g. forward kinematics or inverse kinematics) and the percentage of activation of each skeletal muscle, the computational model can be used to provide the deformation of a group of individual muscles. This resultant deformation can be transmitted to the animal or human skin to produce body deformation. In biomechanics, given a skeletal muscle with a detailed description of the skeletal muscle architecture, the computational model can be used to investigate how forces influence muscle deformation and how deformation affects the contractile properties of muscle.

Previously, we developed a three-dimensional geometric model of skeletal muscle [13] which consists of an assembly of straight lines organized in brick-like elements to represent the skeletal muscle architecture. However, this previously developed model was not sufficiently general to be applied to all possible structural arrangements found in skeletal muscle. Here, we present a non-linear finite element model (FEM) of skeletal muscle based on the theory of continuum mechanics. The model is more general than previously described methods and can be applied for structural arrangements of any shape, and may be applied to other non-linear soft tissues (e.g. tendons) with different material properties. For the geometric representation of the model, we used an assembly of non-uniform brick-

1530-1834/01 $10.00 © 2001 IEEE

like elements. In the nodes of these brick-like elements, we can provide external forces. Muscle deformation can be simulated using displacement control or force control. The model includes the following features: a detailed description of the skeletal muscle architecture; non-linear properties of muscle tissue which allow for large deformations; novel features in the active muscle constitutive equations which may be associated with the percentage of activation of the muscle during specific tasks; and geometric constraints, such as incompressibility and external supports, that can be enforced through Lagrange multipliers.

2 Related Work

In anatomically-based modeling, individual muscles are modeled in an anatomically appropriate way. Scheepers *et al.* [21] presented three anatomy based muscle models, using deformable ellipsoids, Wilhems and Van Gelder [24] used a deformed cylinder model to represent individual muscles, and Nedel and Thalmann [17] presented a model using a line of action approach along with muscle shape, obtained by fitting the surface to the boundary of medical image data. Generally, the anatomy based models present good visual results. However, the proposed models are not robust enough to produce generalized deformations during contraction because of the possible differences in architecture.

In biomechanically-based models, some authors have proposed geometric models of skeletal muscle to represent a detailed skeletal muscle architecture, such as those created by Otten [19], and Van der Linden et al. [23]. Other authors have used physically-based models and finite element models of skeletal muscle, and some other soft tissues. There are many related references regarding biomechanical models for soft tissue simulation which can be found in Maurel *et al.* [15]. Gourret and Thalmann [11] presented a finite element method to grasping simulation, including deformation of the skin of the fingers. Chen and Zeltzer [6] developed a linear finite element model of skeletal muscle in which the simulation of the deformation was performed in a prismatic bounding box embedding the muscle. The resulting muscle deformations were mapped onto the muscle using free-form deformation [22]. Ng-Thown-Hing and Fiume [18] presented a musculoskeletal system using physically-based muscle models along with B-spline solids. Anton and Epstein [1] [2] used a non-linear finite element analysis to simulate two-dimensional unipennate skeletal muscles, including a detailed skeletal muscle architecture. Meier and Blickhan [16] used a non-linear finite element analysis to simulate a three-dimensional skeletal muscle, but the skeletal muscle shape was simplified by a square block. Since one of the goals of this study is to provide methods for the addition of visual realism to the FEM, in order to combine visual and mechanical simulation for use in body deformation visualization, we implemented a stand-alone computational model. This allows us to include our own muscle fibre activation element [13] with novel features in the active muscle constitutive equation.

The excellent early work done by Chen and Zeltzer [6] also includes the twin goal of providing methods to produce realistic skeletal muscle deformation to be used in computer animation applications, and to study muscle function in biomechanical applications. In our study, we include the non-linear properties of muscle tissue in the FEM. None of the previous models include, simultaneously, a detailed description of the three-dimensional skeletal muscle architecture, and a physically consistent model to simulate the deformation behaviour during muscle contraction.

3 Skeletal Muscle Architecture

In order to obtain a detailed description of the skeletal muscle architecture, the geometric representation of the muscle has to support skeletal muscles with different structural arrangements. The structural arrangement of skeletal muscle may be classified into two basic groups according to shape [9]: Parallel-fibred muscles (muscle fibres oriented in parallel to the muscle line-of-action) and pennate-fibred muscles (muscle fibres oriented at a distinct angle relative to the muscle line-of-action). In addition, according to the number of distinctly different fibre directions, pennate muscles are further classified into unipennate muscles (one distinct fibre direction), bipennate muscles (two distinct fibre directions), and multipennate muscles (more than two distinct fibre directions) (Figure 1).

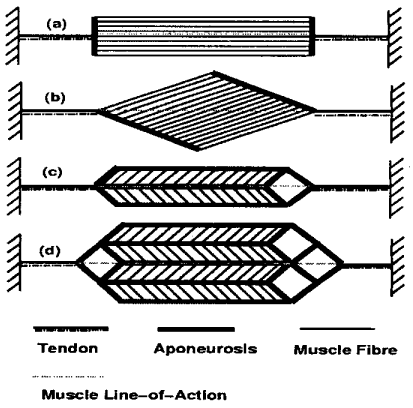

Figure 1: Skeletal muscle shapes. (a) parallel-fibred muscle. (b) unipennate-fibred muscle. (c) bipennate-fibred muscle. (d) multipennate-fibred muscle.

The principal elements of this structural arrangement, which compose the skeletal muscle architecture, are known as the tendon-aponeurosis-fibre complex (Figure 1). The

structural arrangement of this complex describes the mechanism of load transmission, and therefore, muscle deformation during contraction. For example, the force from active contraction elements (muscle fibres) is transmitted to the bone by elastic and viscoelastic tendons and aponeuroses. In addition, the direction of this force is situated in an imaginary straight line (muscle line-of-action) that connects the attachment of the muscle in the bone and the insertion of the tendon in the bone.

For the geometric, three-dimensional representation of skeletal muscle architecture, we adopted an assembly of eight-node brick-like elements. We chose eight-node brick-like elements because in future implementations they will be used as non-uniform hexahedron primitives to generate a polygonal-mesh skin. The model allows for the assembly of brick-like elements next to one another and on top of one another to represent parallel-fibred and pennate-fibred muscles. This structure forms the basis for the non-linear FEM.

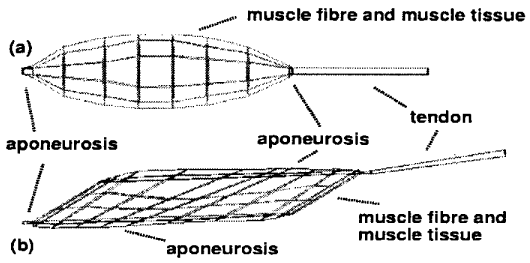

Figure 2: Assembly of brick-like elements. (a) parallel-fibred muscle. (b) unipennate-fibred muscle.

The structural representation of the muscle architecture was obtained through the association of each brick-like element with the biological information that it represents.

The geometric representation of muscle architecture consists of an assembly of four main elements (Figure 2): muscle tissue, aponeurosis tissue, tendon tissue, and muscle fibre tissue. All these separate tissues may be considered as a particular case, represented by a unified brick-like element, which contains an underlying passive tissue matrix. This matrix can be interpreted as a three-dimensional grid with some material inside that provides the internal stability for the muscle fibre assembly and allows for force transmission across muscle fibres. This unified brick-like element can be represented with or without a distribution of unidirectional active muscle fibres, with or without internal incompressibility constraints, and with or without external support constraints. Thus, the elastic material properties [26] can be used to naturally fit the material behaviour.

4 Computational Mechanics Methods for Soft Tissue Simulation

In order to obtain realistic muscle deformations, we formulated a non-linear finite element analysis taking into account experimental data [26] [3] [9] to approximate the behaviour of the materials involved. Following the standard theory of continuum mechanics [5], the formulation consists of three parts: a geometric description of the deformation (or kinematics), a formulation of the equations of motion (or dynamics), and a statement of the behaviour of the materials involved (or constitutive theory). We briefly discuss some aspects of each of these components.

4.1 Kinematics

Adopting, for simplicity, a common global Cartesian coordinate system x, y, and z for both the reference and spatial configurations, and denoting the corresponding displacement components by u, v, and w, the deformation gradient $[\ F\ ]$ is given by the components:

$$[\ F\ ] = [\ I\ ] + \begin{bmatrix} u_{,x} & u_{,y} & u_{,z} \\ v_{,x} & v_{,y} & v_{,z} \\ w_{,x} & w_{,y} & w_{,z} \end{bmatrix} \tag{1}$$

where $[\ I\ ]$ is the unit matrix and commas indicate partial differentiation.

From the deformation gradient we can extract all the information needed about the state of strain by eliminating the rotational component. One way to do this is by calculating the right Cauchy-Green tensor [5] as:

$$[\ C\ ] = [\ F\ ]^T [\ F\ ] \tag{2}$$

A commonly used strain measure [5], sometimes called the Lagrangian strain $[\ E\ ]$, is defined as:

$$[\ E\ ] = \frac{1}{2}(\ [\ C\ ] - [\ I\ ]\ ) \tag{3}$$

which reduces to the ordinary strain measures of the infinitesimal theory when the displacement gradients appearing in equation (1) are small.

In the FEM approach, the continuum is divided into polyhedral elements and the displacement field is approximated by means of nodally-controlled shape functions. In the isoparametric formulation [7], which we adopt, all elements are obtained by mapping a simple prototype repeatedly into the reference configuration. In our treatment, we adopt a cubic prototype with eight nodes located at its vertices ("eight-node brick-like element"; Figure 3). Denoting by ξ, η, and ζ the natural coordinates of the prototype. The shape functions are given by [7]:

$$N_i = \tfrac{1}{8}(1 \pm \xi_i\xi)(1 \pm \eta_i\eta)(1 \pm \zeta_i\zeta) \quad i = 1, \cdots, 8 \tag{4}$$

where ξ_i, η_i and ζ_i are the fixed coordinates of the nodes. By construction, these coordinates can have the values $+1$ or -1 only.

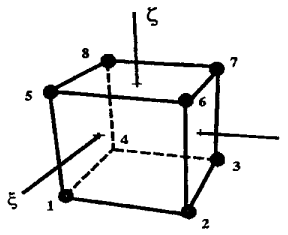

Node	ξ	η	ζ
1	+1	−1	−1
2	+1	+1	−1
3	−1	+1	−1
4	−1	−1	−1
5	+1	−1	+1
6	+1	+1	+1
7	−1	+1	+1
8	−1	−1	+1

Figure 3: Brick-like element with nodal coordinates.

In terms of given global nodal coordinates X^i,Y^i, and Z^i $(i = 1, \cdots, 8)$ in the reference configuration, and given nodal displacements, U^i,V^i, and W^i $(i = 1, \cdots, 8)$, the global coordinates (x, y, and z), and the displacements (u, v, and w) of a point (within the element) with natural coordinates (ξ, η, and ζ), are obtained as:

$$\begin{aligned} x &= \textstyle\sum_{i=1}^{8} X^i N_i(\xi,\eta,\zeta) \quad & u &= \textstyle\sum_{i=1}^{8} U^i N_i(\xi,\eta,\zeta) \\ y &= \textstyle\sum_{i=1}^{8} Y^i N_i(\xi,\eta,\zeta) \quad & v &= \textstyle\sum_{i=1}^{8} V^i N_i(\xi,\eta,\zeta) \\ z &= \textstyle\sum_{i=1}^{8} Z^i N_i(\xi,\eta,\zeta) \quad & w &= \textstyle\sum_{i=1}^{8} W^i N_i(\xi,\eta,\zeta) \end{aligned} \tag{5}$$

To calculate the interpolated deformation gradient, we use the chain rule of differentiation as:

$$[\ F\ ] = [\ I\ ] + \begin{bmatrix} u_{,\xi} & u_{,\eta} & u_{,\zeta} \\ v_{,\xi} & v_{,\eta} & v_{,\zeta} \\ w_{,\xi} & w_{,\eta} & w_{,\zeta} \end{bmatrix} \begin{bmatrix} x_{,\xi} & x_{,\eta} & x_{,\zeta} \\ y_{,\xi} & y_{,\eta} & y_{,\zeta} \\ z_{,\xi} & z_{,\eta} & z_{,\zeta} \end{bmatrix}^{-1} \tag{6}$$

Note that, by virtue of equation (5), the right side of equation (6) is ultimately a well defined function of ξ, η, and ζ.

4.2 Dynamics

The dynamical laws governing the motion of the system are essentially an expression of Newton's second law, except that we have a system with distributed mass rather than just an idealized material particle. In addition, since the internal forces arise from the deformation itself, and since we are not restricting the magnitude of the displacements or rotations, the equations of motion involve angles and distances measured in the unknown deforming configuration. As a result, the equations of motion are highly non-linear. Besides that, geometrical constraints (such as muscle volume preservation) must be respected, and the internal forces necessary to maintain such constraints cannot be easily incorporated into a Newtonian framework.

The non-linear equations of motion are formulated, therefore, by means of the principle of virtual work [9]. For an unconstrained system, this principle states that the equations of motion are equivalent to the satisfaction of the following simple scalar equation:

$$IVW - EVW \equiv 0 \tag{7}$$

identically for all virtual displacement fields δu, δv, and δw. Here IVW and EVW stand, respectively, for internal and external virtual work. The virtual displacement field can be interpreted as a small arbitrary perturbation of a given displacement field, satisfying the support conditions. The internal virtual work within a referential volume V is the work of the internal forces, or stresses, and is given by:

$$IVW = \int_V trace\left([\ T\ ]^T\ [\ \delta F\ ]\right) dV \tag{8}$$

where $[\ T\ ]$ is the first Piola-Kirchhoff stress, equation (10), and $[\ \delta F\ ]$ is the variation of the deformation gradient produced by the virtual displacement [5].

The external virtual work consists of two parts: the work of external forces over the virtual displacements of their points of application, and the work of the distributed inertia forces:

$$EVW = \sum \vec{f} \bullet \delta\vec{u} - \int_V \rho\ddot{\vec{u}} \bullet \delta\vec{u} dV \tag{9}$$

Here, the summation extends over the number of external forces. For convenience, we have employed a vectorial notation for the forces and the displacements. A dot represents the ordinary inner ("dot") product of vectors. The mass density in the reference configuration is denoted by ρ, and the acceleration vector by $\ddot{\vec{u}}$. Currently, the inertia contribution is disregarded, but will be included in future implementations.

In the FEM, expressions such as (8) and (9) can be evaluated element by element. For the eight-node brick-like element, the values of each of these expressions will be controlled by exactly 24 degrees of freedom (3 per node). The principle of virtual work can be modified to take into account geometric constraints by the addition of new variables ("Lagrange multipliers"). Let $\phi(u^1, v^1, w^1, \cdots, u^8, v^8, w^8) = 0$ represent a geometric constraint for a given element (e.g. external support constraint or volume preservation constraint) and let λ denote the corresponding Lagrange multiplier. The internal virtual work of that element is then modified to $IVW - \delta(\lambda\phi)$, where the variation of ϕ is expressed in terms of the nodal displacements and their variations by taking the differential of the constraint function. Thus, the constrained problem is reduced to an unconstrained counterpart but involving more independent

variables (λ) and their corresponding variations ($\delta\lambda$). The physical meaning of the Lagrange multipliers is roughly that of forces necessary to maintain the constraints. The variational method, thus, delivers these forces accurately, avoiding the danger of intuitive considerations.

4.3 Constitutive Behaviour

For the purpose of this paper, we will limit ourselves to general elastic response and disregard viscoelastic effects. For a general elastic material, the constitutive response is expressible as a function relating stresses and strains. A convenient stress measure is the second Piola-Kirchhoff stress represented as:

$$[\ S\ ] = [\ F\ ]^{-1}\,[\ T\ ] \tag{10}$$

A possible constitutive equation consists of relating $[\ S\ ]$ with $[\ E\ ]$, by means of the linear law:

$$[\ S\ ] = 2\,\mu\,[\ E\ ] + \lambda\, trace\,([\ E\ ])\,[\ I\ ] \tag{11}$$

where λ and μ are the Lamé constants of the infinitesimal theory of elasticity [7]. This law is not without problems [10], but is a useful approximation to materials (such as muscle tissue) for which reliable experimental data are not readily available in the very large deformation regime. For the purposes of this paper, we have adopted this constitutive law for all passive tissues (muscle tissue, tendon and aponeurosis) with different values of the Lamé constants. Recall that in infinitesimal elasticity [7], the Lamé constants are related to the Young's modulus, ε, and Poisson's ratio ν by:

$$\mu = \frac{\epsilon}{2(1+\nu)} \quad \lambda = \frac{\epsilon\nu}{(1+\nu)(1-2\nu)} \tag{12}$$

Adopting specific values of these constants for each passive tissue, the contribution for the IVW for a given elastic material element is obtained by plugging equations (10) and (11) into equation (8). We would like to emphasize that any other non-linear elastic constitutive law (such as those of rubber-like materials) can be easily implemented.

As mentioned in Section 3, the active elements are distributed unidirectionally within the muscle tissue. For convenience, this distribution is expressed in terms of a number of fibres per element, so that the number of fibres in contiguous elements can be easily enforced if so desired. Starting from a basic quadratic force-length relationship [9]:

$$f(r) = -0.772r^2 + 1.544r - 0.494 \tag{13}$$

expressing the normal stress in Mpa as a function of the ratio $r = L/L0$ between current, L, and optimal fibre length, $L0$, the force per fibre is assumed to be obtained by:

$$N = a\,[f(r0) + k(r0)(r - r0)] \tag{14}$$

where a is an activation parameter ($0 \leq a \leq 1$) and $r0$ is the value of r upon first activation. The stiffness $K(r0)$, representing the behaviour for active elongations beyond the initial length, is still a matter of controversy, particularly when $r0$ falls on the descending limb of the force-length relationship [8] (Figure 4). The contribution for the IVW of a given active element is obtained by:

$$IVW = \sum N\,\delta e \tag{15}$$

where δe is the small variation in the elongation produced by the virtual displacements of the end points of the active element [13].

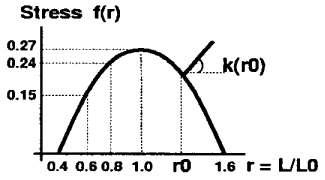

Figure 4: Force response to a stretch upon full isometric activation.

4.4 Computing the Finite Element Scheme

In Figure 5 is shown the pseudocode for computing the finite element scheme for a single skeletal muscle. Numerical solution of the system of non-linear equations derived from the principle of virtual work is achieved by using the Newton-Raphson method [20]. Denoting by $\{p\}$ a vector specifying all positions in the reference configuration of the nodes of the assembly of eight-node brick-like elements, and denoting by $\{u\}$ and $\{\delta u\}$ a vector specifying all the unknowns (nodal displacements and Lagrange multipliers) and their variations, respectively, the main routine computes the function:

$$VW(\{u\},\{\delta u\}) = IVW(\{u\},\{\delta u\}) - EVW(\{u\},\{\delta u\}) \tag{16}$$

where IVW contains the contribution of all brick-like elements for the internal virtual work of a given elastic material element, of a given active element, and of the forces necessary to maintain the constraints ($\delta(\lambda\phi)$). EVW contains the contribution of all brick-like elements for the external virtual work.

To obtain the residual $r_i(\{u\})$ associated with the equation corresponding to the degree of freedom u_i, the function VW is evaluated with all entries for $\{\delta u\}$ equal to zero, except the entry δu_i, which is set to 1. The number of entries

We want to compute, for a given $\{p\}$, the new $\{p\}'$ to establish the new configuration of the geometric skeletal muscle

1. Given
   - (a) The degrees of freedom of the nodes of the brick-like element that are associated with the external supports
   - (b) Either, the position of the external supports as the goal or the load of the external supports as the goal
   - (c) The percentage of activation of the skeletal muscle
   - (d) The initial guess $\{u\}$
2. Compute $\{\Delta u\}$ until the residual $\{r\}$ is lower than a pre-specified admissible error or the maximum number of iterations is reached
   - (a) For each i^{th} entry
     - ($a.1$) Set $\{\delta u\}$ equal to zero except the entry δu_i, which is set to 1
     - ($a.2$) For each brick-like element compute IVW and EVW (only if the current i^{th} entry is associated with that brick-like element)
     - ($a.3$) Compute $r_i(\{u\})$
   - (b) For each i^{th} entry
     - ($b.1$) Set $\{\delta u\}$ equal to zero except the entry δu_i, which is set to 1
     - ($b.2$) For each j^{th} entry
       - ($b.2.1$) Set $\{u\}$ as before except the entry u_j, which is set to $u_j = u_j + h$
       - ($b.2.2$) For each brick-like element compute IVW and EVW (only if the current i^{th} and j^{th} entries are both associated with that brick-like element)
       - ($b.2.3$) Compute $r_i(\{u\}')$
       - ($b.2.4$) Compute $J_{ij} \cong \frac{1}{h}(r_i(\{u\}') - r_i(\{u\}))$
   - (c) Solve the system of linear equations
     $$[\ J\ ]\{\ \Delta u\ \} = -\{\ r\ \}$$
   - (d) Compute $\{u\} = \{u\} + \{\Delta u\}$
3. Compute $\{p\}' = \{p\} + \{u\}$

Figure 5: Pseudocode for computing the finite element scheme.

is always equal to the number of unknowns. The Jacobian matrix J needed for the Newton-Raphson procedure is obtained numerically by the formula:

$$J_{ij} \cong \frac{1}{h}(r_i(\{u\}') - r_i(\{u\})) \tag{17}$$

where $\{u\}'$ is obtained by changing the j^{th} entry of the current vector $\{u\}$ from u_j to $u_j + h$, h being a small number ($h = 0.001$).

The system of linear equations to be solved at each step can be expressed in matrix form as:

$$[\ J\ ]\{\ \Delta u\ \} = -\{\ r\ \} \tag{18}$$

The current displacement vector is updated to $\{u\} + \{\Delta u\}$, and the procedure is repeated until the norm of the residual vector $\{\ r\ \}$ is lower than a pre-specified admissible error.

5 Skeletal Muscle Deformation

The computational model was used to simulate muscle contraction of two ankle extensor skeletal muscles of the cat hindlimb (Figure 6). These muscles are the cat soleus (SOL), a nearly parallel-fibred muscle, and the cat medial gastrocnemius (MG), a perfect unipennate-fibred muscle [12] .

In the computational model, we can specify whether an external support is fixed, partially fixed or free, and whether it is displacement controlled (the goal for the position of the support is specified) or force controlled (the goal for the loads of the support is specified). For the purpose of illustration, we adopted the values $\varepsilon = 250Mpa$, $\varepsilon = 1.7Mpa$, and $\varepsilon = 0.075Mpa$, respectively, for the tendon, aponeurosis and muscle tissue [26]. We assumed $\nu = 0.49$ for all materials, a value which represents volume preserving materials. In order to model other non-linear soft tissues with different material properties, we can simply change the values ε and ν, equation (12).

Figures 7(a) and 8(a) show the initial geometry in the relaxed state that was used as input. Thus, we impose a 2mm displacement at the tendon with the muscle fully activated. The result of the displacement controlled simulations are shown in Figures 7(b)(c) and 8(b)(c). SOL contraction causes a bulging, Figure 7(b)(c), and, MG contraction causes a parallel sliding of the top aponeurosis relative to the bottom one, Figure 8(b)(c).

As a result of the simulation, we can measure fibre lengths, angles of pinnation (angles between the muscle line-of-action and the direction of the muscle fibres), internally developed forces by the muscle fibres and the external force of the whole muscle.

For the case of the SOL model (Figure 7), fibre length at maximal isometric force and muscle length, including the tendon, were assumed to be, respectively, $38.5mm$ and $80mm$ (derived from Herzog *et al.* [12]). And, the maximal

tendon force developed for SOL was $25N$. For the case of the MG (Figure 8), we used the same initial muscle architecture as specified in our previous work [13]. Fibre lengths at maximal isometric force and muscle length, including the tendon, were assumed to be, respectively, $24.5mm$ and $120mm$ (derived from Carvalho *et al.* [4] [3]). Comparisons of external muscle force, fibre lengths, and angles of pinnation were made between theoretically predicted and experimentally measured values [3]. Our previous results [13], and the present results, showed that fibre lengths became smaller (up to about -25%) and angles of pinnation increased (up to about $+20^o$) when going from the relaxed to the activated state in the experiment and the model. The maximal tendon force developed for MG was $128N$. Therefore, since the theoretically predicted results agree with the experimentally measured values the conceptual predictions of the computational model are correct.

In the third example (Figure 9), we used the same conditions as specified in the previous two examples. However, for computer animation purposes or for structure-function relationship explanation purposes, we fully activated only the left side of the muscle. As a result, we obtained a strange deformation. SOL contraction causes a bulging in only half of the muscle, Figure 9(a)(b), and, MG contraction causes torsion and sliding of the top aponeurosis relative to the bottom one, Figure 9(c)(d).

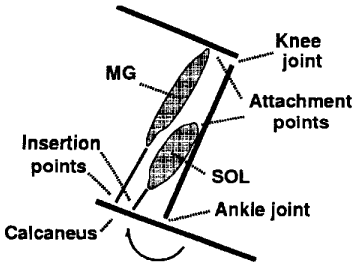

Figure 6: Cat hindlimb.

6 Discussion

The model can be applied to different classes of skeletal muscles according to shape such as parallel-fibred muscles (Figure 7) and pennate-fibred muscles (Figure 8), and may be applied to other non-linear soft tissues with different material properties.

We can experiment with the model in order to discover what happens to it in particular conditions such as to fully activate only the left side of muscle during the muscle contraction (Figure 9). And, the model can be used to investigate how forces influences muscle deformation and how deformation affects the contractile properties of muscle. This investigation is done by taking into account the

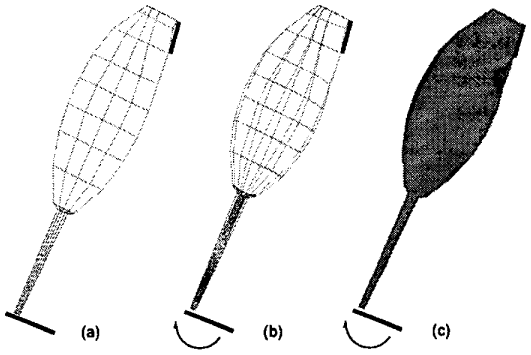

Figure 7: SOL skeletal muscle architecture (a) relaxed state and (b) activated state; SOL polygonal surface (c) activated state.

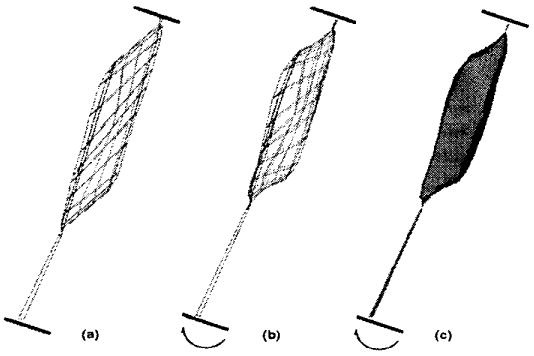

Figure 8: MG skeletal muscle architecture (a) relaxed state and (b) activated state; MG polygonal surface (c) activated state.

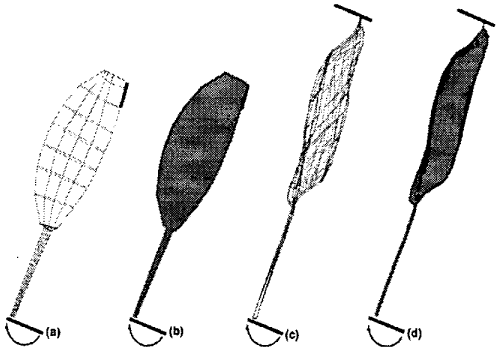

Figure 9: Left side of the muscle activated (a) SOL and (b) SOL polygonal surface; (c) MG and (d) MG polygonal surface.

initial geometry of a particular skeletal muscle architecture, experimental data about the behaviour of the materials involved, and initial conditions about the muscle attachments and tendon insertions.

7 Conclusions and Future Work

We developed a model of skeletal muscle that can be applied for underlying structural arrangements of any shape. The model is sufficiently general for applications in computer animation, and sufficiently accurate to study muscle function in biomechanical applications.

The principle of virtual work, in the presence of geometric constraints, represents a physically consistent model to simulate the deformation behaviour of skeletal muscles. The implementation of a stand-alone computational model in combination with the finite element analysis allows for the inclusion of novel features in the active muscle constitutive equations that eliminate potential instabilities on the descending limb of the force-length relationship in skeletal muscle.

For computer animation, the next steps include realistic modeling and visualization of the skeletal muscle architecture and of the transmission of the resultant deformation, of a group of muscles, to the human or animal skin to produce body deformation. In order to do that we will use implicit and subdivision surfaces modeling techniques [25] [27]. For simulation, the next step includes the implementation of a strategy for the recruitment of groups of muscle fibres during the activation process.

Acknowledgments

CAPES - Brazil, Universidade de Caxias do Sul (UCS), and NSERC of Canada. The first author would like to thank Marcelo Walter and Gladimir Baranoski, for their helpful comments on content.

References

[1] M. Anton. *Mechanical models of skeletal muscle*. Ph.D. dissertation, Dept. of Mechanical Engineering, The University of Calgary, Canada, 1992.

[2] M. Anton and M. Epstein. Continuum model of skeletal muscle tissue. In *8th European Conference on Biomaterials*. European Society for Biomaterials, Heidelberg, 1989.

[3] W. Carvalho. *Structural changes of unipennate muscle during isometric contractions*. Master's thesis, Dept. of Medical Science, The University of Calgary, Canada, 2000.

[4] W. Carvalho, T. Leonard, and W. Herzog. The influence of pinnation and series elasticity on the sarcomere force-length behavior of cat skeletal muscle. In *Canmore Symposium on Skeletal Muscle, Canmore, Canada*, page 42, 1999.

[5] P. Chadwick. *Continuum mechanics concise theory and problems*. Dover Publications, Mineola, New York, 1999.

[6] D. Chen and D. Zeltzer. Pump it up: Computer animation of a biomechanically based model of muscle using the finite element method. *Computer Graphics*, 26(2):89–98, 1992.

[7] R. Cook, D. Malkus, and M. Plesha. *Concepts and applications of finite element analysis*. John Wiley & Sons, New York, 1989.

[8] K. Edman, G. Elzinga, and M. Noble. Residual force enhancement after stretch of contracting frog single muscle fibers. *Journal of General Physiology*, 80:769–784, 1982.

[9] M. Epstein and W. Herzog. *Theoretical models of skeletal muscle*. John Wiley & Sons, Chichester, England, 1998.

[10] M. Epstein and Y. Tene. Nonlinear analysis of pin-jointed space trusses. *American Society of Civil Engineers. Journal of the Structural Division*, 97:2189–2202, 1971.

[11] J. Gourret and N. Magnenat Thalmann. Simulation of object and human skin deformations in a grasping task. *Computer Graphics*, 23(3):21–30, 1989.

[12] W. Herzog, T. Leonard, J. Renaud, J. Wallace, G. Chaki, and S. Bornemisza. Force-length properties and functional demands of cat gastrocnemius, soleus and plantaris muscles. *Journal of Biomechanics*, 25:1329–1335, 1992.

[13] R. Lemos, M. Epstein, W. Herzog, and B. Wyvill. Three-dimensional geometric model of skeletal muscle. In *Skeletal Muscle Mechanics: From Mechanics to Function*, pages 179–206. John Wiley & Sons, 2000.

[14] R. Lieber and J. Fridén. Functional and clinical significance of skeletal muscle architecture. *Muscle & Nerve*, 23:1647–1666, November 2000.

[15] W. Maurel, Y. Wu, N. Magnenat Thalmann, and D. Thalmann. *Biomechanical Models for Soft Tissue Simulation*. Springer-Verlag, Berlin, 1998.

[16] P. Meier and B. Blickhan. Fem-simulation of skeletal muscle: The influence of inertia during activation and deactivation. In *Skeletal Muscle Mechanics: From Mechanics to Function*, pages 207–233. John Wiley & Sons, 2000.

[17] L. Nedel and D. Thalmann. Modeling and deformation of the human body using an anatomically-based approach. *Proceedings of Computer Animation 98*, 1998.

[18] V. Ng-Thow-Hing and E. Fiume. Physically-based modelling of musculoskeletal systems. *Proceedings of Graphics Interface'99*, pages 33–34, 1999.

[19] E. Otten. Concepts and models of functional architecture in skeletal muscle. *Exercise and Sport Sciences Reviews*, 16:89–139, 1988.

[20] W. Press, B. Flannery, S. Teukolsky, and W. Vetterling. *Numerical Recipes in C: the art of scientific computing*. Cambridge, 1988.

[21] C. Scheepers, R. Parent, W. Carlson, and S. May. Anatomy-based modeling of the human musculature. *Computer Graphics*, pages 163–172, 1997.

[22] T. Sederberg and S. Parry. Free-form deformation of solid geometric models. *Computer Graphics*, 20(4):151–160, 1986.

[23] B. van der Linden, H. Koopman, H. Grootenboer, and P. Huijing. Modelling functional effects of muscle geometry. *Journal of Electromyography and Kinesiology*, 8:101–109, 1998.

[24] J. Wilhems and A. Van Gelder. Anatomically based modeling. *Computer Graphics*, pages 173–180, 1997.

[25] B. Wyvill, E. Galin, and A. Guy. Extending the csg tree. warping, blending and boolean operations in a implicit surface modeling system. *Computer Graphics Forum*, 18(2):149–158, 1999.

[26] H. Yamada. *Strength of biological materials*. Willians and Wilkins, Baltimore, MD, 1970.

[27] D. Zorin and P. Schroder. *Subdivision surfaces for modeling and animation*. ACM SIGGRAPH Course Notes, New Orleans, 2000.